Available online at www.sciencedirect.com
ScienceDirect
Magnetic Resonance Imaging 25 (2007) 1196–1202
MAGNETIC RESONANCE IMAGING

A framework for quality control and parameter optimization in diffusion tensor imaging: theoretical analysis and validation

Khader M. Hasan*

Department of Diagnostic and Interventional Imaging, University of Texas Health Science Center at Houston Medical School, Houston, TX 77030, USA

Received 28 November 2006; revised 22 February 2007; accepted 22 February 2007

Abstract

In this communication, a theoretical framework for quality control and parameter optimization in diffusion tensor imaging (DTI) is presented and validated. The approach is based on the analytical error propagation of the mean diffusivity (D_{av}) obtained directly from the diffusion-weighted data acquired using rotationally invariant and uniformly distributed icosahedral encoding schemes. The error propagation of a recently described and validated cylindrical tensor model is further extrapolated to the spherical tensor case (diffusion anisotropy ~0) to relate analytically the precision error in fractional tensor anisotropy (FA) with the mean diffusion-to-noise ratio (DNR). The approach provided simple analytical and empirical quality control measures for optimization of diffusion parameter space in an isotropic medium that can be tested using widely available water phantoms.

Keywords: DTI; FA; Icosahedral encoding; Parameter optimization; DNR; Quality control

1. Introduction

Diffusion tensor imaging (DTI) of water molecular random translational motion is being investigated by many groups as a sensitive and noninvasive method to probe the deep-living tissue organization and microstructure [1]. Although the physiological and morphological contributors to the measured DTI signal are still to be elucidated [2,3], there is a general optimism that DTI can provide important qualitative and rotationally invariant quantitative information about the architecture of living tissue in health and disease [1]. DTI involves the acquisition of large data sets that require the selection of an immense parameter space which has not been clearly investigated with analytical approaches [4–8]. In general, the optimization of the single tensor multi-dimensional parameter problem remains a challenging complex multi-dimensional problem [1,4–15]. The DT-MRI of the entire brain or a certain tissue volume-of-interest is usually sought in some clinically affordable time, T, and a repetition time, T_R. The DTI experiment seeks to acquire a total of $N_T = T/T_R$ images to estimate the diffusion tensor $\boldsymbol{D}$, which is represented as a symmetric 3×3 positive definite matrix ($\boldsymbol{D}_{ij} = \boldsymbol{D}_{ji}$, $i,j = 1,2,3$) with six independent elements (three diagonal and three off-diagonal). A minimum of seven independent measurements are generally needed to encode the tensor [1,4–15]. For example, we can acquire images in the steady state with fixed repetition time (T_R), echo time, (T_E), diffusion time (τ) at multiple diffusion weighting (b-factors), diffusion averaging (N_d), multiple encoding directions (N_e) and/or multiple reference images (N_{ref}). To achieve some level of diffusion sensitization, the b-factor is controlled by the diffusion gradient strength (G_d), the diffusion time and the pulse duration [7,8]. Having $N_T \geq 7$, therefore, provides many possible ways of partitioning the $N_T = N_{ref} + N_d * N_e$.

Despite some progress in DTI processing, acquisition methodologies and applications, the related issues of quality control and parameter selection in DTI remain to be elusive. The availability of some guidelines and analytical methods for the design and testing of DTI protocols would help make DTI more useful in multi-center studies.

In this communication, the special isotropic tensor case (fractional anisotropy FA~0) — which is universally available in the form of spherical water phantoms for quality assessment and control — is shown analytically and experimentally to provide a useful framework for quality control and parameter optimization in DTI.

* Tel.: +1 713 500 7690; fax: +1 713 500 7684.
E-mail address: Khader.M.Hasan@uth.tmc.edu.

0730-725X/$ – see front matter © 2007 Elsevier Inc. All rights reserved.
doi:10.1016/j.mri.2007.02.011

2. Theory

2.1. Computation of D_{av} and RA_n using icosahedral schemes

The relationship between the measured diffusion signals using uniformly distributed icosahedral tensor encoding schemes and the mean diffusivity can be expressed as [16–18]:

$$D_{\mathrm{av}} = <Y> = \frac{\sum_{k=1}^{N_e} y(k)}{N_e} \tag{1}$$

In Eq. (1), $y(k)$ is related to the reference and diffusion-weighted signals as:

$$y(k) = \frac{1}{b}\log\left(\frac{S(0)}{S(k)}\right) = \frac{1}{b}[\log(S(0)) - \log(S(k))], k = 1,2,3,\ldots N_e \tag{2}$$

In this expression, $S(0)$ has been magnitude averaged N_{ref} times to enhance the signal-to-noise ratio (SNR). Assuming independent noise measurements and defining the single image $\mathrm{SNR}_0 = S(0)/\sigma_0$, the SNR in the magnitude-averaged images is expected to increase as, $\mathrm{SNR}(0) = \mathrm{SNR}_0 * \sqrt{N_{\mathrm{ref}}}$. With the use of icosahedral tensor encoding schemes, the normalized relative anisotropy ($\mathrm{RA_n}$) was expressed in terms of the standard deviation of the measurements [16,17].

$$\mathrm{RA_n} = \sqrt{\frac{5}{4}}\sqrt{\frac{1}{N_e}\frac{\sum_{k=1}^{N_e} y(k)^2}{{D_{\mathrm{av}}}^2} - 1}. \tag{3}$$

Standard error propagation can be conducted on both the mean diffusivity and relative anisotropy. With the use of multivariable error propagation rules [18–20], the standard deviation of the multivariable function f of the noise vector η can be expressed in terms of the covariance matrix $\mathrm{Cov}(\eta)$ and first derivative vector [18,19]:

$$\sigma(f(\vec{\eta}))^2 \cong \frac{\partial f(\vec{\eta})^t}{\partial \vec{\eta}}\mathrm{Cov}(\vec{\eta})\frac{\partial f(\vec{\eta})}{\partial \vec{\eta}} \tag{4}$$

Using Eqs. (1), (2) and (4) on a spherical tensor, and assuming independent noise in both the reference (b~0) and diffusion-weighted measurements with standard error $\sigma \sim \sigma_0$ and an SNR in the $b=0$ before magnitude averaging ($\mathrm{SNR}_0 = S(0)/\sigma_0$), we can express the error in D_{av} as:

$$\sigma(D_{\mathrm{av}}) = \frac{1}{b\mathrm{SNR}_0}\sqrt{\frac{1}{N_{\mathrm{ref}}} + \frac{1}{N_T - N_{\mathrm{ref}}}\exp(2bD_{\mathrm{av}})}, \tag{5}$$

In deriving Eq. (5), we have used the fact that $N_d * N_e = N_T - N_{\mathrm{ref}}$ and the fact that for independent noise measurements, $\sigma^2\left(\sum_{k=1}^{N_e} S(k)\right) \cong \sum_{k=1}^{N_e} \sigma^2(S(k))$ and $\sigma^2(\log(S(k))) = \frac{\sigma^2(S(k))}{S(k)^2}$.

Eq. (5) is an exact expression for an isotropic medium or a spherical tensor field (FA~0). The equation, which applies to DTI using icosahedral schemes and subject to the assumption of independent noise measurements, is a generalization of some analogous formulae (see Refs. [5,9] for review) to estimate the apparent diffusion coefficient (ADC) from two sets of measurements. The utility of this formula and its analogous extension to $\sigma(\mathrm{RA_n})$ in DTI parameter optimization (selection of optimal b-factor, and optimal partition N_{ref}/N_T) is discussed below.

2.2. Cylindrical symmetry error propagation formulae for RA_n and D_{av}, $\lambda_{||}$ and $\lambda_\perp$

The axially symmetric tensor [21,22] has two independent eigenvalues with diagonal covariance matrix; hence, the error in the estimated mean diffusivity ($D_{\mathrm{av}}(\lambda_\perp, \lambda_{||}) = \frac{2\lambda_\perp + \lambda_{||}}{3}$) can be expressed using Eq. (4) as:

$$\sigma(D_{\mathrm{av}})^2 \cong \begin{bmatrix} \frac{\partial D_{\mathrm{av}}}{\partial \lambda_{||}} & \frac{\partial D_{\mathrm{av}}}{\partial \lambda_\perp} \end{bmatrix} \begin{bmatrix} \sigma(\lambda_{||})^2 & 0 \\ 0 & \sigma(\lambda_\perp)^2 \end{bmatrix} \begin{bmatrix} \frac{\partial D_{\mathrm{av}}}{\partial \lambda_{||}} \\ \frac{\partial D_{\mathrm{av}}}{\partial \lambda_\perp} \end{bmatrix} \tag{6a}$$

$$\sigma(D_{\mathrm{av}}) = \frac{1}{3}\sqrt{\sigma(\lambda_{||})^2 + 4\sigma(\lambda_\perp)^2} \tag{6b}$$

where we have used the fact that $\frac{\partial D_{\mathrm{av}}}{\partial \lambda_{||}} = \frac{1}{3}$ and $\frac{\partial D_{\mathrm{av}}}{\partial \lambda_\perp} = \frac{2}{3}$.

With the use of the expressions for $\mathrm{RA_n}$ in terms of the ratio $x = \frac{\lambda_{||}}{\lambda_\perp}$ or

$$\mathrm{RA_n} = \frac{\lambda_{||} - \lambda_\perp}{\lambda_{||} - 2\lambda_\perp} = 1 - \frac{3}{x+2} \tag{7}$$

the standard deviation in $\mathrm{RA_n}$ can be expressed as:

$$\sigma(\mathrm{RA_n}) = \frac{\partial \mathrm{RA_n}(x)}{\partial x}\sigma(x) = \frac{\mathrm{dRA_n}}{\mathrm{d}x}\sqrt{\left(\frac{\partial x}{\partial \lambda_\perp}\right)^2 \sigma(\lambda_\perp)^2 + \left(\frac{\partial x}{\partial \lambda_{||}}\right)^2 \sigma(\lambda_{||})^2} \tag{8a}$$

Evaluating the needed derivatives $\frac{\mathrm{dRA_n}}{\mathrm{d}x} = \frac{3}{(2+x)^2}$, $\frac{\partial x}{\partial \lambda_\perp} = -\frac{\lambda_{||}}{\lambda_\perp^2}$, and $\frac{\partial x}{\partial \lambda_{||}} = \frac{\lambda_{||}}{\lambda_\perp}$, we obtain:

$$\sigma(\mathrm{RA_n}) = \frac{1}{3D_{\mathrm{av}}} \times \sqrt{(1-\mathrm{RA_n})^2\sigma(\lambda_{||})^2 + (2\mathrm{RA_n}+1)^2\sigma(\lambda_\perp)^2} \tag{8b}$$

Eqs. (6a,b) and (8a,b) can be expressed in terms of the matrix equation:

$$\begin{bmatrix} \sigma(D_{\mathrm{av}})^2 \\ \sigma(\mathrm{RA_n})^2 \end{bmatrix} = \frac{1}{9{D_{\mathrm{av}}}^2}\begin{bmatrix} 4{D_{\mathrm{av}}}^2 & {D_{\mathrm{av}}}^2 \\ (2\mathrm{RA_n}+1)^2 & (1-\mathrm{RA_n})^2 \end{bmatrix}\begin{bmatrix} \sigma(\lambda_\perp)^2 \\ \sigma(\lambda_{||})^2 \end{bmatrix} \tag{9a}$$

This matrix equation can be inverted to obtain the matrix eigenvalue variance vector:

$$\begin{bmatrix} \sigma(\lambda_\perp)^2 \\ \sigma(\lambda_{||})^2 \end{bmatrix} = \frac{3}{4\mathrm{RA_n}-1}\begin{bmatrix} (1-\mathrm{RA_n})^2 & -{D_{\mathrm{av}}}^2 \\ -(2\mathrm{RA_n}+1)^2 & 4{D_{\mathrm{av}}}^2 \end{bmatrix}\begin{bmatrix} \sigma(D_{\mathrm{av}})^2 \\ \sigma(\mathrm{RA_n})^2 \end{bmatrix} \tag{9b}$$

2.3. Quality control and parameter optimization for DTI

Eqs. (9a,b) can be extrapolated for the extreme isotropic and anisotropic cases of FA=RA_n~0 and FA=RA_n~1, respectively. Note that these formulae predict the errors in the extreme anisotropic case RA_n~1, in which the estimated precision error in RA_n is expected to be dominated by the standard deviation in the perpendicular eigenvalue or $\sigma(\mathrm{RA_n}) \cong \frac{\sigma(\lambda_\perp)}{D_{av}}$.

The standard deviation in the case RA_n~0 ($\lambda_1 \cong \lambda_2 \cong \lambda_3, \lambda_\perp = \frac{\lambda_2+\lambda_3}{2} \Leftrightarrow \lambda_\perp \cong \lambda_\parallel$) can also be expressed as:

$$\sigma(\mathrm{RA_n}) \cong \frac{\sqrt{\sigma(\lambda_\parallel)^2 + \sigma(\lambda_\perp)^2}}{3D_{av}} = \frac{\sqrt{\sigma(\lambda_1)^2 + \sigma(\lambda_2)^2 + \sigma(\lambda_3)^2}}{3D_{av}} \cong \frac{\sigma(D_{av})}{D_{av}} \quad (10a)$$

In this case, λ_2 and λ_3 are correlated and the measurement noise roughens both dimensions, which are consequently expected to contribute at an equal footing. Eq. (10a) can be expressed in terms of the experimental acquisition parameters as:

$$\sigma(\mathrm{RA_n}) \cong \frac{1}{\mathrm{SNR_0 bD_{av}}}\sqrt{\frac{1}{N_{ref}} + \frac{\exp(2D_{av}b)}{N_T - N_{ref}}} \quad (10b)$$

The previous expressions can also be expressed in terms of the more commonly used fractional anisotropy (FA). With the use of the exact relationship between FA and RA_n and its error propagation [18]

$$\mathrm{FA} = \mathrm{RA_n}\sqrt{\frac{3}{1+2\mathrm{RA_n^2}}} \quad (11)$$

$$\sigma(\mathrm{FA}) = \frac{1}{3}\left[\frac{\mathrm{FA}}{\mathrm{RA_n}}\right]^2 \sigma(\mathrm{RA_n}) = \sqrt{3}\left[\frac{1}{1+2\mathrm{RA_n}^2}\right]^{\frac{3}{2}} \sigma(\mathrm{RA_n}) \quad (12)$$

Using Eqs. (10a,b) and (12) and RA_n=FA~0, we can explicitly express the standard deviation in FA as:

$$\sigma(\mathrm{FA}) \cong \sqrt{3}\sigma(\mathrm{RA_n}) = \frac{\sqrt{3}}{\mathrm{DNR(D_{av})}} = \sqrt{3}\frac{\sigma(D_{av})}{D_{av}} \quad (13a)$$

$$\sigma(\mathrm{FA}) \cong \frac{\sqrt{3}}{\mathrm{SNR_0 bD_{av}}}\sqrt{\frac{1}{N_{ref}} + \frac{\exp(2D_{av}b)}{N_T - N_{ref}}} \quad (13b)$$

Eqs. (5), (10a,b) and (13a,b) constitute the basis for the suggested quality control method for DTI using readily and universally available isotropic water phantoms. Eqs. (13a,b) state that for a ghost (image artifact)-free region in an isotropic medium (spherical water phantom), where noise measurements are independent, the error in the mean diffusivity can be predicted as a multivariable function of D_{av}, b, SNR_0, N_{ref} and N_T. Moreover, the measured standard error in FA is inversely proportional to the diffusion-to-noise ratio (DNR), which can be tested experimentally.

2.4. Application of the derived equations to DTI parameter optimization

To the best of our knowledge, these useful and exact formulae have never been derived or published before. The utility of these equations in protocol optimization and DTI experimental design will be briefly considered in this section. For example, the optimal b-factor and partition of the total scan time or number of total acquired image volumes (N_T) can be achieved by requiring for the special case FA~0, $\frac{\partial\sigma_{FA}}{\partial b} = 0$, $\frac{\partial\sigma_{FA}}{\partial N_{ref}} = 0$, for the optimal b-factor and N_{ref} at fixed N_T, or generally $\frac{\partial\sigma(D_{av})}{\partial b} = 0$, $\frac{\partial\sigma(D_{av})}{\partial N_{ref}} = 0$. The simultaneous evaluation of these equations gives a nonlinear equation ($(1-(bD_{av}-1)\exp(bD_{av})=0$) whose optimal bD_{av} solution is given by Eqs. (14a,b,c):

$$b_{optimal} \cong \frac{1.2785}{D_{av}} \quad (14a)$$

$$\left(\frac{N_T}{N_{ref}}\right)_{optimal} \cong 4.5911 \quad (14b)$$

$$\left(\frac{N_d N_e}{N_{ref}}\right)_{optimal} = \exp\left(b_{optimal}D_{av}\right) \cong 3.5911 \quad (14c)$$

For arbitrary partition, the optimal bD_{av} is the solution of the nonlinear equation $\left(1-(bD_{av}-1)\frac{N_{ref}}{N_T}\exp(2bD_{av}\right) = 0$. These results can also be obtained by maximization of the DNR, $\mathrm{DNR} = \frac{D_{av}}{\sigma(D_{av})}$. The maximum achievable DNR(D_{av}) at the optimal b value and partition can be expressed in terms of SNR_0 and the total number of images N_T as:

$$\mathrm{DNR}(D_{av})_{max} = 0.2785{*}\mathrm{SNR_0}\sqrt{N_T} \quad (15a)$$

$$\kappa_D = \frac{\mathrm{DNR(D_{av})_{max}}}{\mathrm{SNR_0}} \cong \sqrt{\frac{N_T}{13}}. \quad (15b)$$

The minimum standard deviation in FA achieved using icosahedral encoding schemes at the optimal b-factor and partition can now be expressed for the isotropic diffusion case as:

$$\sigma(\mathrm{FA})_{min} = \frac{6.219213}{\mathrm{SNR_0}\sqrt{\mathrm{N_T}}}. \quad (16)$$

Note that Eqs. (14a,b,c), (15a,b) and (16) are the DTI analogue of some results presented by Xing et al. [9]. These important results expressed in terms of Eqs. (10a,b), (11), (12), (13a,b), (14a,b,c), (15a,b) and (16) combined with the requirement FA~0 predict that the icosahedral encoding efficiency measured as the DNR(D_{av}) divided by the root of the total time is constant for optimized DTI experiments. These formulae are important in performing b-factor, SNR and quantitative quality control computations. For example, measuring the standard deviation in a

central artifact (ghost) and structure-free water phantom provides a simple and straightforward method for testing the selection of parameters and for evaluating the working SNR_0 as described below.

3. Methods

The theoretical formalism presented above was validated using water phantom DTI measurements (GE spherical water phantom at scanner room regulated temperature) as described previously at 1.5-T [17,18], 3.0-T [6,21,23] and 7.0-T [24] scanners. For DT-MRI data acquisitions at both 1.5 and 3.0 T, the T_E was 60–90 ms, and T_R was 6000–10,000 ms depending on the selected b-factor and slice coverage. The 1.5-T data were acquired using a quadrature coil, whereas the 3.0-T data were acquired using both parallel imaging and quadrature modes. The SNR in the phantom center was computed from replicated independent acquisitions using image absolute mean and difference statistics as illustrated in Results. To facilitate experimental validation of the theoretical predictions, we used an alternating polarity [25], balanced and multi-faceted Icosa21bpn [23,24] with many N_{ref} and diffusion-weighted averages, b-factors, etc., at room temperature. The choice of Icosa21bpn encoding scheme gave many rotationally invariant subsets that enabled time-efficient validation of the theoretical predictions from the same acquired data [24]. The data acquisition, residual eddy current distortion correction and processing details are described elsewhere [1,4,18,23,26].

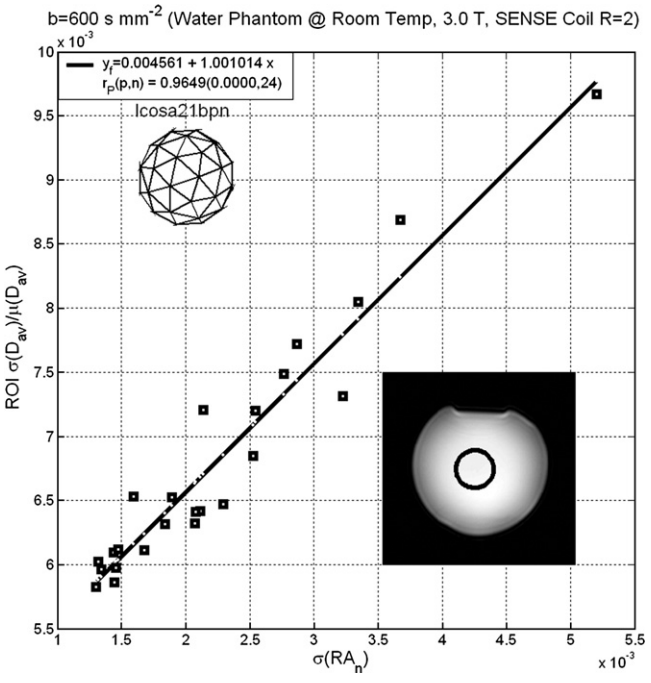

Fig. 1. Experimental demonstration and validation of the model presented on a water phantom at 3.0 T of the predicted theoretical relationship between the ROI standard error in RA_n and the inverse of the mean DNR. The plot shows the results of 24 different experiments acquired using the Icosa21bpn scheme at different total number of images, N_{ref}, N_d and N_e but constant b-factor (b-factor=600 s mm^{-2}). The encoding scheme and ROI are also shown. The plot shows the Pearson correlation coefficient and the corresponding best fit and P values.

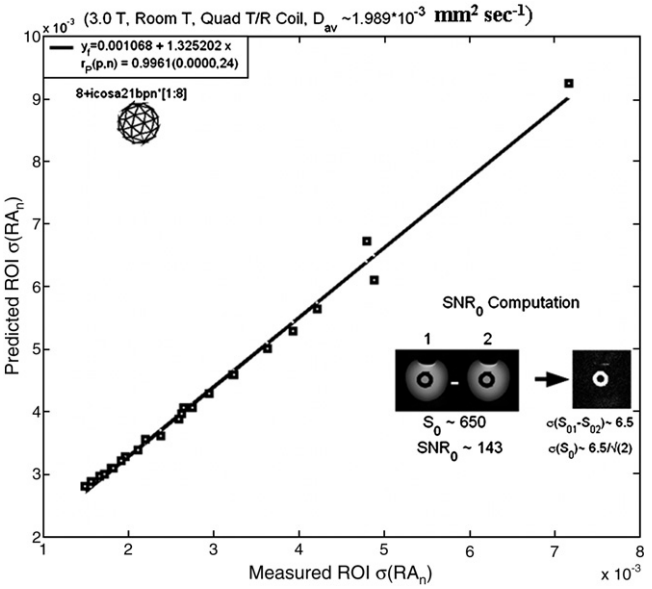

Fig. 2. Experimental demonstration on a water phantom at 3.0 T of the relationship between the measured $\sigma(RA_n)$ and the predicted values using our theoretical analysis (Eqs. (10a,b)). The plot shows the results of 24 different experiments acquired using different subsets of Icosa21bpn scheme at different total number of images, N_{ref}, N_d and N_e, but constant b-factor (b-factor=600 s mm^{-2}). The encoding scheme, ROI and SNR_0 estimation method are also shown (see brief description in Methods). Notice that SNR_0 was estimated from the mean of two sets with N_{ref}=1, and variance in the difference images. The estimated mean diffusivity is consistent with known values at the estimated room temperature (see Ref. [1] for more details).

4. Results

Fig. 1 shows an experimental validation of the theoretical relation derived in the manuscript between the standard deviation in RA_n and the inverse of the mean DNR. The data were collected at 3.0 T using a spherical phantom from a large DTI data pool (24 data sets) collected using the alternating polarity (Icosa21bpn) scheme with different N_{ref} and N_d(N_T=N_{ref}+N_d*N_e). Large and central regions-of-interest (ROIs~600 voxels) devoid of any image artifacts were used to estimate the mean and standard errors in the mean diffusivity, FA and RA_n. Using large but homogeneous ROIs ensured spatial noise independence. Notice the striking correlation (Pearson correlation r=0.965, P<.00001; ~unity slope) of the measured $\sigma(RA_n)$ and the inverse DNR(D_{av}) as the theory or Eq. (10a) predicted. Fig. 2 shows the results using another data pool (24 experiments) acquired at 3.0 T from a spherical water phantom. The plot shows the measured $\sigma(RA_n)$ vs. the predicted values using the theoretical formalism or Eq. (10b) above. Notice the ability of our model to predict the standard deviation dependence on many parameters (b-factor, D_{av}, N_{ref}, N_d, encoding scheme and N_e), once

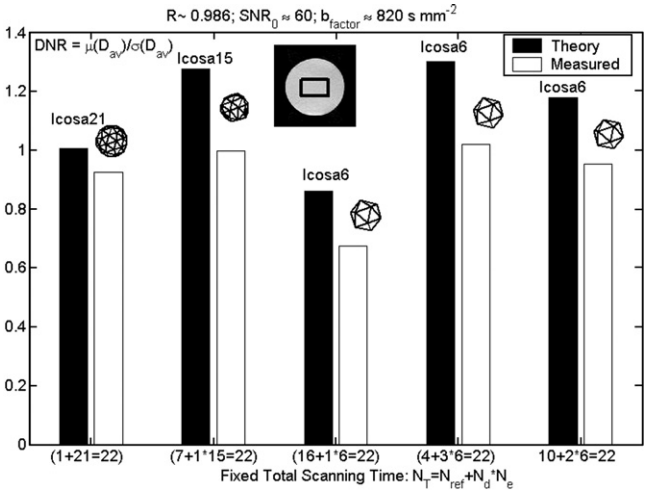

Fig. 3. A bar plot comparison of the predicted vs. measured mean DNR (DNR(D_{av})) for different encoding subsets of Icosa21b using different combinations of N_{ref}, N_d and N_e, but constant N_T=22. The data set was acquired at 1.5 T, with an SNR_0=60 (using one reference image or N_{ref}=1) and a b-factor=820 s mm^{-2}. Notice the strong correlation between the measured and predicted values (r=0.986); the slight deviation of the measured from the predicted values is attributed to the computation of SNR_0, which may fluctuate for different images due to scanner stability (compare these results with the theory in Table 1 and Fig. 4).

more attesting the validity of the theory (r=0.996; P=.000). Since the relation between $\sigma(RA_n)$ and DNR(D_{av}) involves estimating SNR_0, we also illustrate the method used at 3.0 T which involved the subtraction of two identical images since background noise using sensitivity-encoded imaging would not have facilitated direct background noise estimation [23,27]. Fig. 3 compares the measured and predicted DNR(D_{av})/SNR_0 on a water phantom acquired at 1.5 T at constant total scan time. Different combinations of N_{ref}, N_d, and N_e (Icosahedral schemes — Icosa6, Icosa15 and Icosa21) were used keeping N_T=22. Note the ability to predict the DNR(D_{av})/SNR_0 using the theoretical model presented (r=0.986; P<.0001). On this water phantom, the largest DNR(D_{av})/SNR_0 is observed using the combination N_T=22=4+Icosa6*3, which gives a ratio of N_e*N_d/N_{ref} closest to the theoretical maximum predicted in Eqs. (14a,b,c). Note that only discrete numbers for the tensor encoding scheme were used (N_e=6, 15 and 21), yet we are able to predict using Eq. (10b) that this is the closest to the theoretically achievable maximum DNR/SNR_0 as detailed in Table 1 for N_T=20 and N_T=22. Fig. 4 shows a theoretical plot of the κ_D=DNR(D_{av})/SNR_0 vs. $\xi=b*D_{av}$ for different combinations of N_{ref} and N_d*N_e, and constant N_T=22=N_{ref}+N_d*N_e using different encoding schemes, Icosa6, Icosa16 and Icosa21. Using N_T=22, the maximum κ_D=DNR(D_{av})/SNR_0 is predicted to be satisfied by the Icosa6 with N_{ref}=4 and N_d=3 (compare with Table 1 and the experimental results in Fig. 3).

The theoretical model derived in this work was also applied to predict the tabulated water phantom data in some earlier reports [10,24]. In particular, the model predicted successfully the tabulated data in both Madi et al. (see Table 2 and Fig. 1 in Ref. [24]) and Jones et al. (see Table 6 in Ref. [10]).

5. Discussion and conclusions

In this work, we started with the simple but widely used single tensor model [1–5]. Icosahedral DTI encoding schemes were adopted in this report to reduce biases introduced due to encoding sampling [5,6,15–17] and to enable the error propagation of the mean diffusivity expression derived from the measured encoded raw data [16,17]. This work has also presented the propagation of error in the axial tensor described recently [21] and used the special case (FA~0) to provide an analytical formalism for DTI quality control that can be tested experimentally on widely available spherical water phantoms. The spherical tensor used in our formalism could not be handled asymptotically using analytical or perturbation theoretical methods attempted previously [9–14]. Note that Eqs. (10a,b) and (13a,b) predict the expected residual anisotropy error reported using DTI Monte Carlo simulations [11,13,18] (and references therein).

Table 1
Optimal partition of equal time acquisition table for N_T=20, 22

Encoding scheme	N_e	N_T	N_{ref}	N_d	$N_d/N_e/N_{ref}$	κ=DNR(D_{av})/SNR_0 (theory)
XYZ	3	22	1	7	21	1.0063
			4	6	4.500	1.3005
			7	5	2.1429	1.2768
			13	3	0.6923	1.0405
			19	1	0.1579	0.6129
Icosa6	6	22	16	1	0.3750	*0.8596*
			10	2	1.2000	1.1796
			4	3	4.5000	1.3005
Icosa10	10	22	2	2	10.0000	1.1949
			12	1	0.8333	1.0911
Icosa15	15	22	7	1	2.1429	1.2768
Icosa15	15	20	5	1	3	1.2419
Icosa16	16	20	4	1	4	1.2441
Icosa16	16	22	6	1	2.6667	1.2963
Icosa21	21	22	1	1	21	1.0913

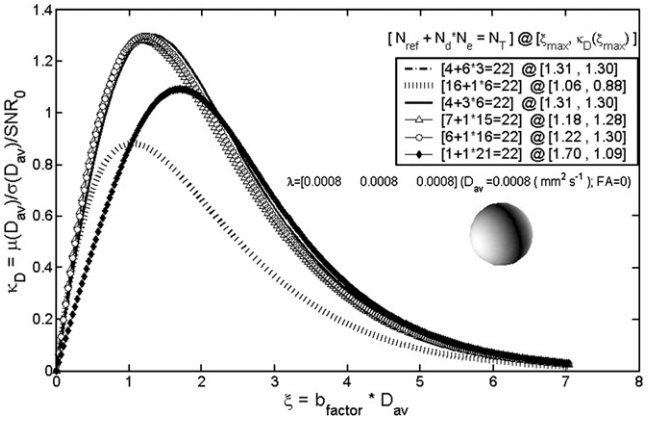

Fig. 4. Illustration of the empirical (theoretical) DT-MRI optimization results at equal time for an isotropic tensor (FA=0, D_{av}=0.0008 mm^2 s^{-1}). The plots show the optimal κ_D and $\xi_{max}=b_{opt}*D_{av}$ as a function of $\xi=b*D_{av}$ at constant total imaging time, $N_T=22=N_{ref}+N_d*N_e$ (compare with Table 1 and Fig. 3) and for different combinations (N_{ref}, N_d*N_e) using different encoding schemes, XYZ, Icosa6, Icosa15, Icosa16 and Icosa21. The tensor eigenvalues $\lambda_{1,2,3}$=[0.0008, 0.0008, 0.0008] mm^2 s^{-1}. Note that the maximum DNR is associated with Icosa6 with $N_{ref}=4$, $N_d=3$. The increase in $b_{opt}*D_{av}$ as N_d*N_e/N_{ref} deviates from the optimal theoretical ratio ~3.6 is also demonstrated.

In the Theory section, we have implicitly assumed that temporal and spatial stability of the MRI measurements warrant SNR enhancement by the temporal multiplexing upon magnitude averaging by the root of the number of excitations or $\sqrt{}$NEX [27]. In our experimental validation, magnitude averages were used with large ROIs to reduce the influence of spatial and temporal fluctuations [27]. The discrepancy between the measured (experimental) and predicted (theoretical) values (see regressed slope and intercept in Figs. 2 and 3) is attributable to the noise statistical variability in the measurement of SNR(0), which requires both spatial and temporal stability (see Ref. [27] for details). The use of uniformly and isotropically distributed icosahedral schemes is justified as no apriori knowledge on the distribution of tensor orientations in space is assumed, especially for the spherical tensor case used in the theory; this warrants using uniformly distributed and icosahedral encoding schemes [5,10,11,15–18].

In this paper, we presented an analytical expression for the error in the spherical tensor noise-sensitive case as an asymptotic limit of the cylindrical tensor (Eqns. (10)–(16)) and demonstrated its utility experimentally at different magnetic field strengths, different alternating polarity multi-faceted icosahedral schemes and different b-factors, N_d and N_{ref} (Figs. 1–3).

This paper also suggests a theoretical SNR efficiency and equivalence of parameter selection using optimized icosahedral schemes at equal time (see Eq. (16)). This theoretical equivalence was also demonstrated by Alderman et al. [28] in 1990 in the context of the analogous chemical shield tensor parameter optimization and sensitivity analysis of the chemical shield anisotropic tensor case. Alderman et al. [28] concluded "Interestingly, the figures of merit show that measuring for a unit of time at 6 icosahedron vertex directions is just as sensitive as measuring for the same total time at 10 or 15 apolar directions defined by the icosahedron faces and edges because of the simplicity of employing 6 rather than 10 or 15 directions, the icosahedron vertex directions are clearly the best choice."

The isotropic water phantom measurements presented here, DTI bootstrap experiments [17,18] and Monte Carlo simulations presented previously at equal time [11] support this notion. In practice, scanner temporal stability is hard to achieve and cannot be fulfilled experimentally for finite samples, thus temporal averaging at small number of excitations (NEX) may not reduce the noise standard error by the theoretical value $\sqrt{}$NEX [27]. On the other hand, a large number of scans have to be averaged to achieve the central limit requirement. Alternatively, replicated temporal averaging can be replaced at equal scan time with acquisitions at higher angular resolution maintaining the optimal partition requirements.

The theoretical framework presented in this work can be used to predict the tabulated measurements using water phantoms [10,24,29]; (see also data in Table 2 and Fig. 1 collected at 7 T in Ref. [24]). It is also noteworthy that the relationship (Eq. (10a)) between the precision error in anisotropy and the coefficient of variation in mean diffusivity (inverse of DNR) has been anticipated using random noise distribution analysis as described in the Appendix of Hirsch et al. [30]. The approach adopted in this work derived that relationship without appealing to random noise distribution models [30]. The theoretical and experimental results presented in this work are somewhat discrepant with those presented in Ref. [10] on the spherical phantom (FA~0), which predicted a higher optimal ratio of N_d*N_e/N_{ref}~8–12. Nevertheless, our theoretical model can predict "in the least squares sense" the relationship between the tabulated σ(FA) vs. $\sigma(D_{av})/D_{av}$ (i.e., using H_2O data from Table 6 in Ref. [10]; $r(\sigma(FA), \sigma(D_{av})/D_{av})=0.9973$; $P=.0027$; $n=4$) but not the graphical plots (Fig. 4 in Ref. [10]). Note that the results in Ref. [10] were derived using numerical error propagation of the anisotropic tensor case and could not asymptotically predict the spherical tensor case which is known to be degenerate using the theoretical perturbation approach presented in by Anderson [12]. In conclusion, the theoretical analysis presented in this work is intended to provide some practical quality control measures to help in the design of efficient longitudinal DTI protocols for multi-center clinical trials. The generalization of our validated framework (FA~0) to arbitrary anisotropy values (FA>0) and the application to human brain measurements in both gray and white matter is beyond the scope of this communication and will be considered in a future manuscript.

Acknowledgments

This work is funded by the National Institute of Neurological Disorders and Stroke (NINDS) NIH-Grant R01-

NS052505 to KMH (Diffusion Tensor Imaging of Wallerian Degeneration in Multiple Sclerosis). The assistance of Marci A. Harris in editing the manuscript and Vipul Kumar Patel in water phantom data collection at 3.0 T is also appreciated. I wish also to thank and acknowledge the support of Drs. Jack M. Fletcher, Michael Boska, Linda Ewing-Cobbs, Joel L. Steinberg, Gerry F. Moeller, Larry A. Kramer, Andrew Papanicolaou, Susan John and Ponnada A. Narayana.

References

[1] Le Bihan D. Diffusion and perfusion magnetic resonance imaging — applications to functional MRI. New York: Raven Press; 1995.
[2] Beaulieu C. The basis of anisotropic water diffusion in the nervous system — a technical review. NMR Biomed 2002;15:435–55.
[3] Norris DG. The effects of microscopic tissue parameters on the diffusion-weighted magnetic resonance imaging experiment. NMR Biomed 2001;4:77–93.
[4] Basser PJ, Mattiello J, Le Bihan D. Estimation of the effective self-diffusion tensor from the NMR spin echo. J Magn Reson B 1994;103: 247–54.
[5] Conturo TE, McKinstry RC, Aronovitz JA, Neil JJ. Diffusion MRI: precision, accuracy and flow effects. NMR Biomed 1995;8:307–32.
[6] Hasan KM. Fundamentals of diffusion tensor imaging of the entire human brain: review of basic theory, data acquisition, processing and potential applications at 1.5 T and 3.0 T. In: Chen FJ, editor. Progress in brain mapping research. Hauppauge (NY): Nova Science Publishers; 2006. pp. 1–80.
[7] Stejskal EO, Tanner JE. Spin diffusion measurements: spin echoes in the presence of a time-dependent field gradient. J Chem Phys 1965; 42:288–92.
[8] Price WS. Pulsed-field gradient nuclear magnetic resonance as a tool for studying translational diffusion: experimental aspects. Concepts Magn Reson 1998;10:197–237.
[9] Xing D, Papadakis NG, Huang CLH, Lee VM, Carpenter TA, Hall LD. Optimized diffusion weighting for measurement of apparent diffusion coefficient (ADC) in human brain. Magn Reson Imaging 1997;15:771–84.
[10] Jones DK, Horsfield MA, Simmons A. Optimal strategies for measuring diffusion in anisotropic systems by magnetic resonance imaging. Magn Reson Med 1999;42:515–25.
[11] Hasan KM, Parker DL, Alexander AL. Comparison of optimization procedures for diffusion-tensor encoding directions. J Magn Reson Imaging 2001;13:769–80.
[12] Anderson AW. Theoretical analysis of the effects of noise on diffusion tensor imaging. Magn Reson Med 2001;46:1174–88.
[13] Pajevic S, Basser PJ. Parametric and non-parametric statistical analysis of DT-MRI data. J Magn Reson 2003;161:1–14.
[14] Poonawalla AH, Zhou XJ. Analytical error propagation in diffusion anisotropy calculations. J Magn Reson Imaging 2004;19:489–98.
[15] Batchelor PG, Atkinson D, Hill DL, Calamante F, Connelly A. Anisotropic noise propagation in diffusion tensor MRI sampling schemes. Magn Reson Med 2003;49:1143–51.
[16] Akkerman EM. Efficient measurement and calculation of MR diffusion anisotropy images using the platonic variance method. Magn Reson Med 2003;49:599–604.
[17] Hasan KM, Narayana PA. Computation of the mean diffusivity and fractional anisotropy maps without tensor decoding and diagonalization: theoretical analysis and experimental validation. Magn Reson Med 2003;50:589–98.
[18] Hasan KM, Alexander AL, Narayana PA. Does fractional anisotropy have better noise immunity characteristics than relative anisotropy in diffusion tensor MRI? An analytical approach. Magn Reson Med 2004;51:413–7.
[19] Bevington PR, Robinson DK. Data reduction and error analysis for the physical sciences. 2nd ed. New York: McGraw-Hill; 1992.
[20] Fukunaga K. Introduction to statistical pattern recognition. San Diego: Academic Press; 1990.
[21] Hasan KM, Narayana PA. Retrospective measurement of the diffusion tensor eigenvalues from diffusion anisotropy and mean diffusivity in DTI. Magn Reson Med 2006;56:130–7.
[22] Conturo TE, McKinstry RC, Akbudak E, Robinson BH. Encoding of anisotropic diffusion with tetrahedral gradients: a general mathematical diffusion formalism and experimental results. Magn Reson Med 1996;35:399–412.
[23] Jaermann T, Crelier G, Pruessmann KP, Golay X, Netsch T, van Muiswinkel AM, et al. SENSE-DTI at 3 T. Magn Reson Med 2004; 51:230–6.
[24] Madi S, Hasan KM, Narayana PA. Diffusion tensor imaging of in vivo and excised rat spinal cord at 7 T with an icosahedral encoding scheme. Magn Reson Med 2005;53:118–25.
[25] Neeman N, Freyer JP, Sillerud LO. A simple method for obtaining cross-term free images for diffusion anisotropy studies in NMR microimaging. Magn Reson Med 1991;21:138–43.
[26] Hasan KM, Basser PJ, Parker DL, Alexander AL. Analytical computation of the eigenvalues and eigenvectors in DT-MRI. J Magn Reson 2001;152:41–7.
[27] Weisskoff RM. Simple measurement of scanner stability for functional NMR imaging of activation in the brain. Magn Reson Med 1996;36: 643–5.
[28] Alderman DW, Sherwood M, Grant D. Two-dimensional chemical-shift tensor correlation spectroscopy: analysis of sensitivity and optimal measurement directions. J Magn Reson 1990;86:60–9.
[29] Hunsche S, Moseley ME, Stoeter P, Hedehus M. Diffusion-tensor MR imaging at 1.5 and 3.0 T: initial observations. Radiology 2001;201: 550–6.
[30] Hirsch JG, Bock M, Essig M, Schad LR. Comparison of diffusion anisotropy measurements in combination with the flair-technique. Magn Reson Imaging 1999;117:705–16.